Mice with targeted *Slc4a10* gene disruption have small brain ventricles and show reduced neuronal excitability

Stefan Jacobs*, Eva Ruusuvuori†, Sampsa T. Sipilä†‡, Aleksi Haapanen§, Helle H. Damkier¶, Ingo Kurth*, Moritz Hentschke*, Michaela Schweizer‖, York Rudhard‖, Linda M. Laatikainen†, Jaana Tyynelä§, Jeppe Praetorius¶, Juha Voipio†, and Christian A. Hübner*,**,†,‡‡

*Department of Human Genetics and ‖Zentrum für Molekulare Neurobiologie Hamburg, University of Hamburg, D-20249 Hamburg, Germany; †Department of Biological and Environmental Sciences, University of Helsinki, 00014 Helsinki, Finland; ‡Department of Clinical Neurophysiology, Helsinki University Central Hospital, FIN-00290 Helsinki, Finland; §Experimental MRI Laboratory, Department of Neurology, Institute of Biomedicine/Biochemistry Biomedicum, University of Helsinki, Helsinki University Central Hospital, FIN-00290 Helsinki, Finland; ¶Water and Salt Research Center, Institute of Anatomy, University of Aarhus, DK-8000 Aarhus C, Denmark; and **Department of Clinical Chemistry, Friedrich-Schiller-Universität, Erlanger Allee 101, D-07747 Jena, Germany

Edited by Peter C. Agre, Duke University, Durham, NC, and approved November 14, 2007 (received for review June 12, 2007)

Members of the SLC4 bicarbonate transporter family are involved in solute transport and pH homeostasis. Here we report that disrupting the *Slc4a10* gene, which encodes the Na^+-coupled Cl^-–HCO_3^- exchanger Slc4a10 (NCBE), drastically reduces brain ventricle volume and protects against fatal epileptic seizures in mice. In choroid plexus epithelial cells, Slc4a10 localizes to the basolateral membrane. These cells displayed a diminished recovery from an acid load in KO mice. Slc4a10 also was expressed in neurons. Within the hippocampus, the Slc4a10 protein was abundant in CA3 pyramidal cells. In the CA3 area, propionate-induced intracellular acidification and attenuation of 4-aminopyridine-induced network activity were prolonged in KO mice. Our data indicate that Slc4a10 is involved in the control of neuronal pH and excitability and may contribute to the secretion of cerebrospinal fluid. Hence, Slc4a10 is a promising pharmacological target for the therapy of epilepsy or elevated intracranial pressure.

cerebrospinal fluid | epilepsy | ion transport | knockout mouse | pH regulation

The *SLC4A10* gene encodes an Na^+-dependent Cl^-–HCO_3^- exchanger (NCBE), SLC4A10 (1), that belongs to the subgroup of Na^+-coupled HCO_3^- transporters of the *SLC4* gene family (2). The importance of this gene family is highlighted by its association with human diseases, such as hemolytic anemia, renal tubular acidosis, and corneal dystrophy (3, 4). SLC4A10 utilizes the transmembrane gradient of Na^+ to drive cellular net uptake of HCO_3^- (or CO_3^{2-}) and thus mediates acid extrusion. Thereby, SLC4A10 may play an important role in intracellular pH (pH_i) regulation in various kinds of cells. In the choroid plexus, SLC4A10 is strongly expressed within the basolateral membrane of epithelial cells (5–7), suggesting a role in transepithelial electrolyte transport and production of cerebrospinal fluid (CSF). In previous studies, the mRNA has been primarily detected in the brain, including the hippocampus (1, 7, 8), but the protein distribution in the CNS has not been resolved.

Commonly, a rise in brain pH is associated with increased neuronal excitability, whereas a fall in pH has been shown to have the opposite effect (9, 10). Recently, hyperthermia-induced respiratory alkalosis was demonstrated to trigger ictal activity in a febrile seizure model (11). In genetic studies, disruption of the related *Slc4a3* gene encoding the neuronal Cl^-–HCO_3^- exchanger Ae3 (Slc4a3), which mediates an efflux of bicarbonate, drastically reduced seizure threshold in mice (12). Furthermore, a common polymorphism within the coding sequence of *SLC4A3* is associated with human idiopathic generalized epilepsy (13). Intracellular acidification, in contrast, is known to facilitate termination of epileptiform activity (14).

Because numerous HCO_3^- transporters are expressed in the CNS and no SLC4A10-specific inhibitors are available, the role of SLC4A10 in physiological and pathophysiological processes has been difficult to examine. In the present work, we disrupted the gene-encoding Slc4a10 in mice. This mouse model suggests important functions of Slc4a10 in the production of the CSF, as well as in the control of neuronal excitability.

Results

Generation of Slc4a10 KO Mice. The targeting strategy for the generation of Slc4a10 KO mice resulted in the deletion of exon 12 of the *Slc4a10* gene (Fig. 1*A*), which encodes the first of the predicted 11–13 transmembrane spans of Slc4a10. This leads to a frameshift and a premature termination codon in exon 13. Homologous recombination was verified by Southern blot analysis with a 3′ probe by using an additional SpeI site in the targeted allele. Two independent, correctly targeted ES cell clones were injected into blastocysts and gave heterozygous offspring. Heterozygous mice showed no obvious phenotype. From heterozygous matings, homozygous KO mice were born in the expected Mendelian ratio (≈25%). In mixed litters on a regular diet, most of the KO pups died around weaning (27 of 34 KO pups monitored) [supporting information (SI) Fig. 6*A*]. When fed soft food from the second week of life onward, most KO pups finally caught up to the weight of their WT and heterozygous littermates and survived (SI Fig. 6 *A* and *B*). In small ($n < 7$ pups) KO litters from KO matings, body weight gain, under normal diet, was not retarded (SI Fig. 6*C*). Adult KO mice had a normal weight and lifespan. They were fertile, and the carriage was to term.

From a multiple-tissue Northern blot, it was obvious that *Slc4a10* is prominently expressed in the CNS (SI Fig. 7*A*). Northern blot analysis of total brain RNA with a Slc4a10-cDNA probe demonstrated the absence of a transcript in KO

Author contributions: S.J., E.R., and S.T.S. contributed equally to this work; J.T., J.P., J.V., and C.A.H. designed research; S.J., E.R., S.T.S., A.H., H.H.D., I.K., M.H., M.S., Y.R., L.M.L., J.P., and C.A.H. performed research; C.A.H. contributed new reagents/analytic tools; S.J., E.R., S.T.S., A.H., H.H.D., I.K., M.H., M.S., Y.R., L.M.L., J.T., J.P., J.V., and C.A.H. analyzed data; and E.R., S.T.S., J.P., J.V., and C.A.H. wrote the paper.

The authors declare no conflict of interest.

This article is a PNAS Direct Submission.

††Present address: Department of Clinical Chemistry, Friedrich-Schiller-Universität, Erlanger Allee 101, D-07747 Jena, Germany.

‡‡To whom correspondence should be addressed. E-mail: christian.huebner@med.uni-jena.de.

This article contains supporting information online at www.pnas.org/cgi/content/full/0705487105/DC1.

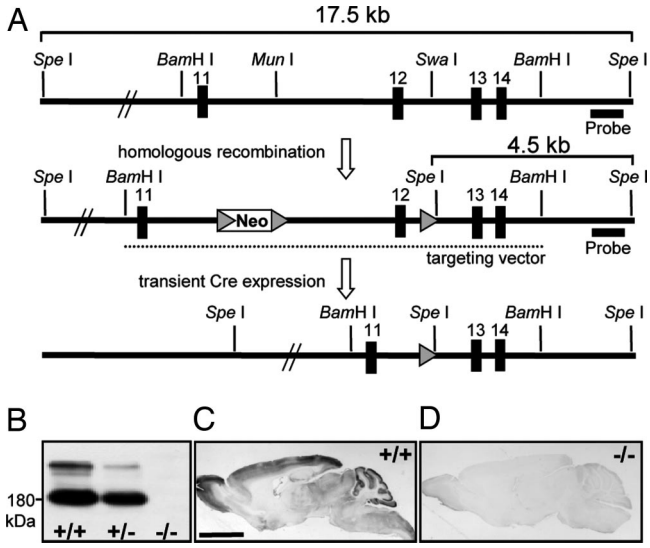

Fig. 1. Generation of Slc4a10 KO mice. (*A*) (*Top*) Partial genomic structure of the *Slc4a10* gene. (*Middle*) Targeted Slc4a10 locus. Dotted line represents the extent of the homology region of the targeting construct. A neomycin selection cassette flanked by loxP sites (gray arrowheads) was inserted into intron 11. A third loxP site was introduced into intron 12. Two correctly targeted ES cell clones were transiently transfected with a Cre-recombinase expression plasmid. (*Bottom*) ES cell clones with a Cre-mediated excision of the DNA fragment between the outer loxP sites were subsequently used for the generation of chimeric mice. (*B*) A membrane protein immunoblot with an Slc4a10 antibody confirmed the absence of Slc4a10 in brain tissue of KO mice. (*C*) In DAB stainings of sagittal brain sections, Slc4a10 localizes to the choroid plexus, cortex, olfactory bulb, cerebellum, brainstem, and spinal cord, but is not detected in large fiber tracts as the corpus callosum. (*D*) The specificity of the staining was confirmed by its absence in KO tissue.

mice (SI Fig. 7*B*). Transcript analysis of *Slc4*, *Slc9*, *Slc12*, and *Slc26* family members, known to transport chloride, bicarbonate, or protons (2, 15–18), did not reveal compensatory changes in expression levels in Slc4a10 KO mice (SI Fig. 7*C*).

Slc4a10 KO Mice Do Not Display Major Behavioral Deficits. To characterize the role of Slc4a10 in learning and behavior, KO mice were subjected to behavioral tests. A major hearing impairment was excluded by an unaltered startle response to acoustic stimuli. Overall locomotor activity did not substantially differ between the genotypes (SI Fig. 8 *A* and *B*). Major alterations in motor coordination were excluded by the rotarod test (SI Fig. 8*C*). In the light–dark test, KO mice spent slightly more time in the bright area, compared with WT (SI Fig. 8*D*). The habituation of exploratory locomotion within new surroundings was delayed in KO mice (SI Fig. 8 *E* and *F*), as was exploratory activity in response to a new object (data not shown). To investigate spatial learning abilities, which are thought to depend on the integrity of the hippocampus, KO mice were subjected to the Morris water maze (SI Fig. 8 *G* and *H*). Both WT and KO mice learned to reach the platform in an efficient manner. With the platform removed from the pool, the mice spent significantly more time swimming and searching within the learned goal location, with no significant difference between the genotypes. Hence, disruption of Slc4a10 did not entail major behavioral abnormalities.

Localization of the Slc4a10 Protein in the Mouse CNS. To detect Slc4a10 at the protein level, a polyclonal antiserum against an N-terminal epitope of murine Slc4a10 was raised in rabbits. In protein lysates of WT brains, the affinity-purified antibody detected an ≈180-kDa band that was absent in KO tissue (Fig. 1*B*). Diaminobenzidine (DAB) stainings (Fig. 1 *C* and *D*) showed that Slc4a10 was broadly expressed in the olfactory bulb, cortex, and cerebellum (Fig. 1*C*). Fiber tracts, such as the corpus callosum or white matter of the spinal cord, did not stain for Slc4a10. The specificity of the antibody and the staining procedure were further confirmed by the absence of the signal in KO tissue (Fig. 1*D*). Double-staining immunofluorescence demonstrated that there was no overlap of Slc4a10 with cells positive for 2′,3′-cyclic nucleotide 3′-phosphodiesterase (CNPase) (SI Fig. 9 *A–C′*), which is a marker of oligodendrocytes, or glial fibrillary acidic protein (GFAP) (SI Fig. 9 *D–F′*), which is a marker of astrocytes. In accordance with the neuronal expression pattern of Slc4a10 in the CNS, the protein was only detected in protein lysates of mixed neuron/glia cell cultures, but not in lysates of glia cell cultures (SI Fig. 9*G*). Double staining for glutamic acid decarboxylase (GAD) and Slc4a10 indicated that some neocortical interneurons expressed Slc4a10 (SI Fig. 10 *A–C*), whereas in the cerebellum, Slc4a10 expression was abundant in Purkinje cells stained for parvalbumine, but absent in interneurons of the molecular layer (SI Fig. 10 *D–F*).

Brain Ventricle Size Is Drastically Reduced in Slc4a10 KO Mice. We confirmed that Slc4a10 did not colocalize with the apical Na^+/K^+-ATPase, but was expressed at the basolateral side of choroid plexus epithelial cells as described previously (Fig. 2*A*) (5, 6). The signal was absent in tissue from KO mice (Fig. 2*B*). Because the choroid plexus is involved in CSF production, we performed MRIs of brains in anesthetized WT (Fig. 2*C*) and KO (Fig. 2*D*) mice to see whether the deletion of Slc4a10 would be associated with anatomical changes *in vivo*. A prominent change was observed in the volume of ventricles, which was drastically diminished in KO mice (10.49 ± 1.8 mm^3 in WT mice, $n = 3$; 2.31 ± 0.39 mm^3 in KO mice, $n = 4$; $P = 0.002$; calculated from T_1-weighted 3D FLASH manganese-enhanced MRI scans) (Fig. 2 *C–E*). Collapsed ventricles could be a sign of increased intracranial pressure and accumulation of water in the brain parenchyma. However, except for the diminished volume of ventricles, other anatomical alterations usually associated with increased pressure were not observed. Furthermore, T_2 and apparent diffusion coefficient (ADC) values, which correlate with tissue water content (19), were not increased. Averaged for the whole-brain, T_2 was diminished by −8.1% in KO ($n = 3$), compared with WT ($n = 4$) mice ($P = 0.03$), whereas ADC was not significantly changed (SI Table 1 and SI Fig. 11). Together these data provide evidence against the possibility that edema would lead to increased intracranial pressure and thereby to the small ventricle size in the brains of Slc4a10 KO mice. Histological analysis showed that the choroid plexus appeared to float in CSF in WT mice (SI Fig. 12*A*), whereas it touched the walls of the ventricles in KO mice (SI Fig. 12*B*). EM further revealed that lateral intercellular spaces were enlarged and apical microvilli drastically reduced in KO tissue (Fig. 2 *F* and *G*).

To address the role of Slc4a10 in pH regulation in the choroid plexus, clusters of choroid plexus epithelial cells were isolated and acid-loaded by an ammonium pulse (Fig. 2*H*). No recovery of pH_i was seen in WT controls when the ammonium washout was done by using saline devoid of Na^+ for up to 2 min ($n = 6$). When Na^+ was reapplied at the time of peak acidification (KO, 6.54 ± 0.05, $n = 5$; WT, 6.53 ± 0.05, $n = 6$; $P = 0.9147$), the subsequent and immediate Na^+-dependent recovery of pH_i in the presence of bicarbonate was diminished in KO (0.0058 ± 0.0010 s^{-1}; $n = 5$), compared with WT mice (0.0191 ± 0.0045 s^{-1}; $n = 6$; $P = 0.028$) (Fig. 2 *H* and *I*). These data suggest that basolateral Na^+ entry by Slc4a10 (Fig. 2*J*) may be involved in Na^+ secretion and, hence, in the production of the CSF.

Region- and Cell-Specific Slc4a10 Expression in the Hippocampus. Histological analysis of brains of 6-month-old Slc4a10 KO mice did not show any gross morphological changes (demonstrated for the hippocampus in SI Fig. 12 *C–F*). DAB immunostaining

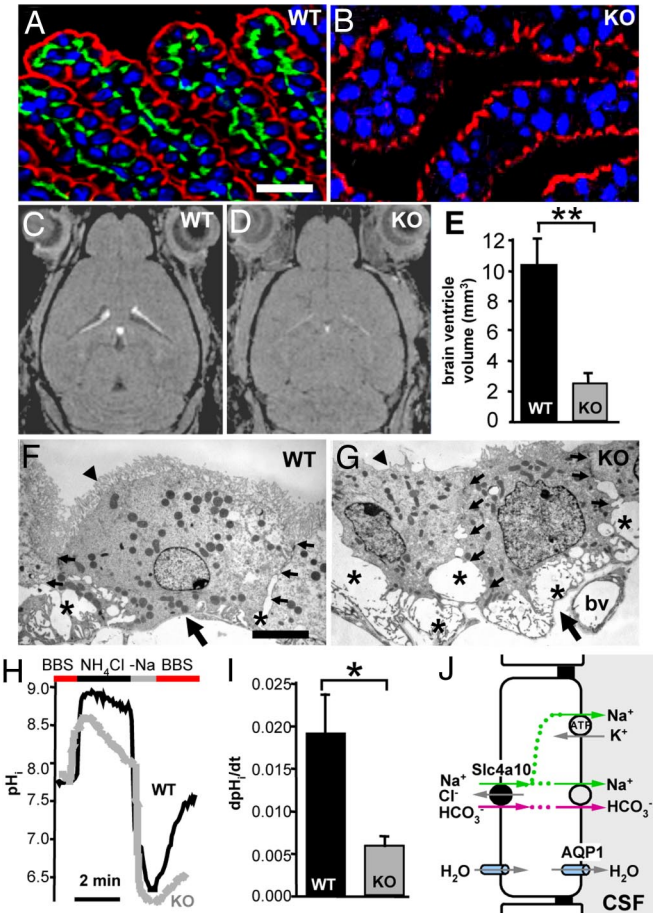

Fig. 2. Deletion of Slc4a10 induces changes in the structure and function of choroid plexus epithelial cells and reduces the volume of brain ventricles. (*A*) Slc4a10 (green) specifically localizes to the basolateral, but not the apical, membrane stained for the Na^+/K^+-ATPase (red) of the choroid plexus epithelium. (*B*) Specificity of the signal was confirmed by its absence in the choroid plexus tissue from KO mice. (*C* and *D*) In T_1-weighted 3D FLASH manganese-enhanced MRI scans, fluid-filled space appears dark and choroid plexus appears white. (*E*) Volume of brain ventricles was subsequently calculated from WT ($n = 3$) and KO ($n = 4$) mouse brains. In KO mice, it was reduced to ≈25% of the WT volume (mean ± SEM). **, $P < 0.01$. (*F* and *G*) Ultrastructural analysis of the KO choroid plexus epithelium (*G*) revealed enlarged lateral intercellular spaces (*) and a reduction of apical microvilli (arrowheads), compared with WT (*F*). Small arrows mark lateral cell borders, whereas large arrows mark the basal cell pole. bv, blood vessel. (*H*) Representative recordings of pH_i from individual cells of choroid plexus from WT and Slc4a10 KO mice. Cells equilibrated in bicarbonate-buffered salt solution (BBS) were acidified by an NH_4Cl pulse, which was washed out by Na^+-free media (−Na). (*I*) Rate of Na^+-dependent pH_i recovery (dpH_i/dt) was measured after readdition of Na^+ (BBS) at the time of peak acidosis. dpH_i/dt was calculated from the slopes of the respective curves (mean dpH_i/dt ± SEM; WT, $n = 6$; KO, $n = 5$). *, $P < 0.05$. (*J*) Proposed model for the secretion of CSF. Na^+ enters the choroid plexus epithelial cells at the basolateral side mainly by Slc4a10. It is secreted apically by Na^+-bicarbonate cotransport and the Na^+/K^+-ATPase. Water follows passively by aquaporin 1 water channels. (Scale bars: *A* and *B*, 30 μm; *F* and *G*, 1 μm.)

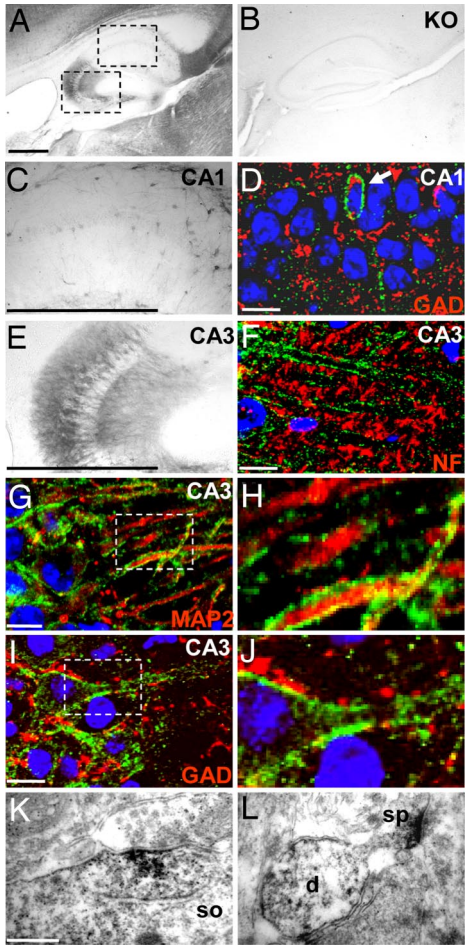

Fig. 3. Cellular and subcellular localization of Slc4a10 in hippocampus. (*A*) DAB stainings of the hippocampus reveal that Slc4a10 is abundant in the CA3 region (sagittal). The dashed frames indicate the regions displayed at higher magnifications in *C* and *E*. (*B*) Staining was absent in KO tissue. (*D*) Some Slc4a10-positive cells were identified as interneurons because of their expression of GAD. (*E*) In CA3, the stratum oriens, stratum pyramidale, stratum radiatum, and lacunosum moleculare stained positive for Slc4a10. (*F–H*) Slc4a10 did not localize to axons stained for NF (*F*) but localized to MAP2-stained dendrites of pyramidal cells (*G* and *H*). (*I* and *J*) Slc4a10 was often closely associated with GAD, a presynaptic marker of inhibitory interneurons. (*K* and *L*) In electron micrographs of DAB-stained sections of the CA3 region, somata (so) (*K*), dendrites (d) (*L*), and spines (sp) were stained. (Scale bars: *A*, 0.5 mm; *C* and *E*, 1 mm; *D*, *F*, *G*, and *I*, 5 μm; *K*, 500 nm.) Slc4a10 is shown in green; MAP2, NF, and GAD are shown in red; nuclei are stained in blue.

revealed a regional difference in Slc4a10 expression between CA1 and CA3 in the hippocampus. Contrary to a lower expression level seen in CA1, higher levels of Slc4a10 were detected in somata and the basal and apical dendrites of pyramidal cells of the CA3 region (Fig. 3 *A–E*). Slc4a10 also was prominently expressed in somata and dendrites of interneurons identified by their expression of GAD as displayed for CA1 (Fig. 3*D*). There was no overlap of Slc4a10 with glia cell markers or neurofilament 68 (NF), which stains axons (Fig. 3*F*).

Slc4a10 was associated with microtubule-associated protein 2 (MAP2)-positive dendrites of CA3 pyramidal cells (Fig. 3 *G* and *H*), and it was partially juxtaposed with GAD, a presynaptic marker of inhibitory neurons (Fig. 3 *I* and *J*). In electron micrographs of DAB-stained sections of CA3 (Fig. 3 *K* and *L*), Slc4a10 appeared to be localized to somatic (Fig. 3*K*) and dendritic (Fig. 3*L*) synapses. However, because the peroxidase reaction product is diffusible and tends to deposit at sites of high protein concentration, the ultrastructural localization of Slc4a10 needs to be addressed in future studies by using ImmunoGold labeling.

Neuronal pH_i Regulation Is Compromised in Slc4a10 KO Mice. The role of Slc4a10 in hippocampal CA3 pyramidal cell pH regulation was examined by using BCECF fluorescence imaging. The baseline pH_i did not differ in slices from Slc4a10 KO mice (7.11 ± 0.02, $n = 12$ slices from seven animals), compared with WT (7.08 ± 0.04, $n =$

NEUROSCIENCE

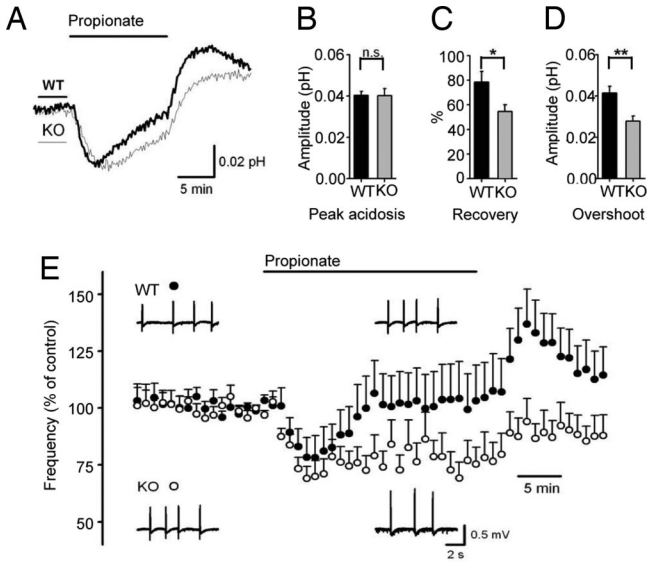

Fig. 4. An exogenous acid load reveals a defect in pH_i regulation in Slc4a10 KO slices with a parallel in network activity. (*A*) Grand averages of pH_i responses upon an intracellular acid load induced by bath application of 20 mM propionate for 13 min (horizontal bar) from CA3 stratum pyramidale (12 Slc4a10 KO slices, gray line; 10 WT slices, black line). Upward deflections indicate an increase in pH_i. (*B–D*) Mean ± SEM values of the peak acid shift in pH_i induced by propionate (*B*), recovery of pH_i in percentage of peak acidosis by the end of the propionate application (*C*), and amplitude of the alkaline overshoot during propionate washout (*D*). *, $P < 0.05$; **, $P < 0.01$. (*E*) Effect of 10 mM propionate on the occurrence of 4-AP-induced interictal-like events in WT (filled circles; $n = 20$ slices) and Slc4a10 KO slices (open circles; $n = 27$ slices) shown as a relative mean (+ SEM) frequency calculated from a sliding 3-min time window. (*Insets*) Sample traces of interictal-like events recorded with field potential electrodes in the hippocampal CA3 pyramidal cell layer under control conditions (*Left*) and during 25-min propionate application (*Right*) in the WT (*Upper*) and Slc4a10-KO (*Lower*) slices.

10 slices from six animals; $P = 0.37$). Bath application of 20 mM propionate (for 13 min) induced an acid shift with an identical peak amplitude in KO and WT slices (0.040 ± 0.0034 and 0.040 ± 0.0018, respectively; $P = 0.97$) (Fig. 4 *A* and *B*). The rate of pH_i recovery during the propionate exposure was significantly faster in the WT ($\Delta pH_i/\Delta t$: 0.0050 ± 0.00037 pH units per min^{-1}) than in KO CA3 pyramidal cells (0.0036 ± 0.00034 pH units per min^{-1}; $P = 0.023$), resulting in a nearly complete pH_i recovery in WT slices by the end of the propionate exposure ($P = 0.027$) (Fig. 4*C*). Accordingly, the alkaline overshoot upon propionate washout was more pronounced in WT than KO slices (0.041 ± 0.0034 vs. 0.028 ± 0.0025, respectively; $P = 0.0022$) (Fig. 4*D*).

pH Regulation by Slc4a10 Is Involved in the Control of Network Excitability. The manifestation at the level of network phenomena of disrupted Slc4a10 expression was studied by using the *in vitro* 4-aminopyridine (4-AP) model. Bath application of 50 μM 4-AP induced interictal-like events at 0.02–1.4 Hz in field potential recordings from the CA3 stratum pyramidale. Subsequent application of 10 mM propionate caused a peak decrease in the frequency of the interictal-like events within ≈6 min to 75 ± 10% ($n = 20$ slices from four animals) and to 66 ± 6% ($n = 27$ slices from four animals) in WT and KO slices, respectively, with no statistically significant difference between the two genotypes ($P = 0.41$) (Fig. 4*E*). Although the frequency of the interictal-like events recovered to the control level (101 ± 14% of the control value; $P = 0.92$) in WT slices, the frequency in the KO slices was significantly below (74 ± 7%; $P = 0.001$) the control value at ≈14 min from the beginning of the propionate application. This result shows a striking similarity with the time

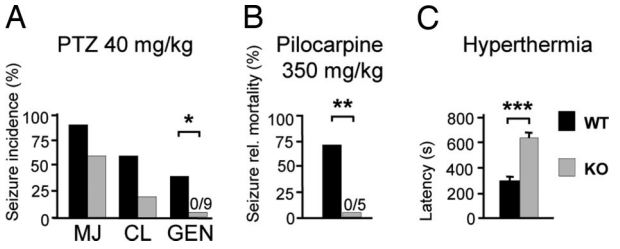

Fig. 5. Slc4a10 KO mice have a higher seizure threshold. (*A*) After i.p. injection of PTZ, Slc4a10 KO mice did not experience generalized seizures (GEN) (WT, $n = 10$; KO, $n = 9$). MJ, myoclonic jerk; CL, clonic seizure. (*B*) KO mice were protected against fatal epileptic activity after induction of generalized epileptic activity by pilocarpine. (*C*) Onset of hyperthermia-induced generalized epileptic activity in 10-day-old KO pups was significantly delayed. Shown are means + SEM. *, $P < 0.05$; **, $P < 0.01$; ***, $P < 0.001$.

courses of the pH_i responses described earlier. Furthermore, washout of propionate induced a rebound increase in the network event frequency in the WT slices, but not in the KO slices. At ≈6 min from the beginning of the washout, the frequency was 137 ± 15% and 94 ± 10% of the control value in the WT and KO slices, respectively ($P = 0.02$). These *in vitro* data indicate that Slc4a10 is involved in the control of excitability of the hippocampal CA3 network, and that this action of Slc4a10 is likely mediated by its contribution to the regulation of pH_i.

Slc4a10 KO Mice Have an Increased Seizure Threshold. Given the important role of pH on neuronal excitability, we tested the susceptibility of Slc4a10 KO mice to proconvulsant substances. In Slc4a10 KO mice, the latency until onset of myoclonic jerks (MJ) after application of 40 mg/kg pentylenetetrazole (PTZ) was almost doubled (299 ± 42 s; $n = 6$), compared with WT (154 ± 33 s; $n = 9$; $P = 0.026$). Epileptic activity did not further progress to generalized seizures (GEN) (Fig. 5*A*). At a higher dose (60 mg/kg), all KO mice recovered from epileptic activity, whereas 9 of the 18 WT mice ($P = 0.00078$) died. The influence of Slc4a10 on mortality also was obvious after administration of pilocarpine (Fig. 5*B*). Although five of seven WT mice died because of generalized epileptic activity, all KO mice survived ($n = 5$; $P = 0.008$).

Hyperthermia causes ictal activity because of hyperventilation and a concomitant rise of intracranial pH in a rat pup model of febrile seizures (11). The latency until the onset of generalized seizures was more than doubled in Slc4a10 KO mice ($n = 8$), compared with WT mice ($n = 10$; 627 ± 15 s and 278 ± 18 s, respectively; $P = 0.0000014$) of comparable body weight (KO, 5.02 ± 0.11 g; WT, 4.92 ± 0.15 g; $P = 0.62$) (Fig. 5*C*). All except two WT pups rapidly recovered from epileptic activity. Taken together, disruption of Slc4a10 increases the seizure threshold in a variety of seizure-inducing paradigms.

Discussion

To address the physiological functions of the NCBE, we disrupted the *Slc4a10* gene in mice. KO mice are viable and show no major behavioral abnormalities. However, KO mice have smaller brain ventricles, compared with the WT animals, and display an increased threshold to experimentally induced seizures. At the cellular level, Slc4a10 was found to be involved in pH regulation of choroid plexus epithelial cells and neurons, as well as in the modulation of neuronal excitability.

Our antibody revealed that Slc4a10 was expressed in various regions of the brain in a cell-type-specific manner. Double labeling with glial markers GFAP and CNPase, as well as immunoblot detection of Slc4a10 from cell cultures, showed that neurons, but not glial cells, express Slc4a10. In the hippocampus, Slc4a10 was abundant in the somata and dendrites of interneu-

rons and CA3 pyramidal cells. Electron micrographs localized Slc4a10 to dendritic membranes within the stratum oriens and stratum radiatum. We also confirmed the previously reported basolateral localization of Slc4a10 in choroid plexus epithelial cells (5, 6).

The production of CSF by the epithelial cells of the choroid plexus largely depends on apical Na^+ secretion by the Na^+/K^+-ATPase, a yet unidentified basolateral Na^+ loader, and osmotic flow of H_2O by aquaporin 1 (20). In this study, we demonstrated that Na^+-dependent acid extrusion is severely diminished in choroid plexus epithelial cells of Slc4a10 KO mice, suggesting that the basolaterally expressed Slc4a10 is the main Na^+-dependent transporter regulating pH_i in these cells. Furthermore, MRI scans of the brain showed that the volume of brain ventricles was drastically diminished in Slc4a10 KO mice. T_2 and ADC maps calculated from MRI scans excluded the possibility of edema and increased water content in the brains of Slc4a10 KO mice. Taken together, these data suggest that a failure in the CSF production is likely to cause the collapse of brain ventricles in these mice. Although here an Na^+-dependent acid/base transporter proves to be necessary for the bulk of epithelial secretory or absorptive processes, it is obvious that other transport mechanisms operate in parallel with Slc4a10. Na^+-dependent acid extrusion was not completely blocked in choroid plexus epithelial cells from Slc4a10 KO mice. The anion transporter inhibitor DIDS causes only a partial inhibition of solute transport or CSF production (6, 21). Furthermore, the carbonic anhydrase inhibitor, acetazolamide, has been shown to inhibit CSF production rate or Na^+ secretion (20, 22, 23). The close proximity between transporter and enzyme has been shown to be necessary for the optimal function of several SLC4A family members (24). These results propose that the transepithelial solute transport mediated by Slc4a10 is involved in serious clinical conditions, such as brain edema and hydrocephalus.

Slc4a10 was strongly expressed in CA3 pyramidal neurons that are well known for their propensity to generate physiological sharp waves, as well as pathological interictal events (25–29). Propionate application caused a transient decrease in the pH_i in the WT CA3 pyramidal neurons and, with a similar time course, a suppression of 4-AP-induced interictal-like activity. This finding suggests that the slower pH_i recovery detected in the Slc4a10 KO slices during an exogenous acid load fully accounts for the prolonged suppression of the 4-AP-induced interictal-like activity in the concomitant electrophysiological recordings. Hence, Slc4a10 works against acid shifts when CA3 pyramidal neurons are challenged by an endogenous acid load during intense neuronal activity, and the observation provides further support for a key role of Slc4a10 in pH-dependent modulation of neuronal excitability. The compromised ability to extrude acid most likely causes the higher seizure threshold observed in Slc4a10 KO mice in experiments with proconvulsant substances, as well as in the rodent pup model of febrile seizures. This conclusion gains additional support from the observation that the deletion of the Cl^-–HCO_3^- exchanger Ae3, which imposes an intracellular acid load by HCO_3^- efflux, is associated with an increased sensitivity to seizure-inducing agents (12). These data stipulate that SLC4A10 may be a target for anticonvulsant drugs, and SLC4A10 may be considered a potential modifier in human seizure disorders. As the gene localizes to the 2q23–2q24 region, which includes the *SCN1A* and *SCN2A* genes mutated in monogenic epilepsy syndromes (30, 31), it is tempting to speculate that gain-of-function mutations in *SLC4A10* may contribute to the disorder in families without *SCN1A* mutations.

Is a change in neuronal HCO_3^- uptake consistent with the observed differences in the pH-dependent effects on neuronal excitability between Slc4a10 KO and WT slices? pH_i modulates neuronal activity by a variety of mechanisms, including those involved in GABAergic and glutamatergic transmission (10). For instance, $GABA_A$ receptor channels mediate a significant net efflux of HCO_3^- under physiological conditions (32, 33), and an increase in pH_i induces an increase in the depolarizing bicarbonate current component in ionotropic GABAergic responses (34). Furthermore, the depolarizing action of HCO_3^- efflux by $GABA_A$ receptors drives a conductive net uptake of chloride, resulting in chloride-mediated positive shifts in $GABA_A$ receptor responses (35). A rapid replenishment of intraneuronal HCO_3^- stores has been shown to be crucial for a nonsynaptic excitatory action of GABA (36). Finally, intracellular acidosis attenuates synaptic glutamatergic responses, which involve direct effects of pH on membrane proteins (10, 37). Thus, a defect in neuronal HCO_3^- uptake may lead to a reduction in excitability by a number of mechanisms.

In summary, our mouse model reveals that the Na^+-dependent anion exchanger Slc4a10 plays an important role in pH_i regulation and, thereby, affects pH-dependent modulation of neuronal excitability. This ion transporter also is intimately involved in solute transport in choroid plexus epithelial cells, and thus it is likely to contribute to the secretion of CSF. Hence, SLC4A10 may be a drug target in the therapy of epilepsy and increased intracranial pressure.

Experimental Procedures

Experiments were approved by the responsible local institutions and complied with the regulations of the National Institutes of Health and those of the Society of Neuroscience. Experimenters were blinded to the genotype.

Generation of Slc4a10 KO Mice. The *Slc4a10* gene was disrupted by homologous recombination in ES cells and blastocyst injection as detailed in *SI Methods*. Mice were maintained on a 12-h artificial light–dark cycle and provided with food and water ad libitum.

Northern Blot Analysis and Quantitative RT-PCR. Northern blot analysis and quantitative RT-PCR were performed as described in refs. 38 and 39, respectively. Primer sequences are available upon request.

Antibody Generation and Western Blot Analysis. The Slc4a10 antiserum was raised in rabbits against the epitope KHRKRDRERDSGLED (amino acids 71–85 of the Slc4a10 protein; accession no. NM 033552), coupled by a C-terminal cysteine to keyhole limpet hemocyanin and affinity-purified. Mixed neuron/glia cell cultures or glia cell cultures were performed as described in ref. 40. For Western blotting, 10 μg of membrane-enriched protein fraction was separated on reducing SDS/7.5% PAGE. Blots were probed with the rabbit Slc4a10 antibody at a dilution of 1:250. Detection was done with the chemoluminescence ECL-Kit (Amersham Biosciences).

Morphology. For details of histology, immunocytochemistry, and EM, see *SI Methods*.

Behavioral Tests. Male mice were housed individually in standard transparent laboratory cages. The activity, light–dark, rotarod, open field, and Morris water maze assay is described in detail in *SI Methods*. The experiments started when the animals were 3 to 4 months old and weighed 25–35 g. Tests were performed during the light phase between 10:00 a.m. and 5:00 p.m.

Seizure Susceptibility. Seizures were evoked by administration of the chemical proconvulsants, pentylenetetrazole or pilocarpine, or by hyperthermia. Peripheral cholinergic actions of pilocarpine were blocked with methylscopolamine. For details, see *SI Methods*.

Electrophysiology and pH_i Fluorescence Imaging. For details on field potential recordings and BCECF fluorescence imaging of pH_i from hippocampal CA3 stratum pyramidale and isolated choroid plexus epithelial cells, see *SI Methods*.

MRI Analysis. Brain ventricle volume, brain water content, and apparent diffusion coefficient maps were obtained from anesthetized mice by MRI methods (described in detail in *SI Methods*).

Statistical Analysis of Data. All numerical data are expressed as mean ± SEM. Statistical tests used for analyses of data are given in *SI Methods*.

ACKNOWLEDGMENTS. We thank Kai Kaila, T. J. Jentsch, and A. Dityatev for discussions and valuable comments on the manuscript; I. Hermans-Borgmeyer and A. Hübner for continuous support; and H. Jahn for hosting S.J. for the behavioral analysis of mice. This work was supported by German Research Foundation Grants SFB 444, HU 800/3–1, FOR 604, and GRK 336 (to C.A.H.); the Novo Nordisk Foundation; the Danish Medical Research Council; the University of Aarhus Research Foundation; Karen Elise Jensen Fonden; the Faculty of Health Science, University of Aarhus (J.P.); the Academy of Finland (J.V. and J.T.); University of Helsinki Research Funds (J.V.); the Finnish Funding Agency for Technology and Innovation (J.V.); the Sigrid Juselius Foundation (J.V.); the Ella and George Ehrnrooth Foundation (E.R.); and the Paulo Foundation (S.T.S.).

1. Wang CZ, Yano H, Nagashima K, Seino S (2000) *J Biol Chem* 275:35486–35490.
2. Romero MF, Fulton CM, Boron WF (2004) *Pflügers Arch* 447:495–509.
3. Vithana EN, Morgan P, Sundaresan P, Ebenezer ND, Tan DT, Mohamed MD, Anand S, Khine KO, Venkataraman D, Yong VH, *et al.* (2006) *Nature Gen* 38:755–757.
4. Alper SL (2002) *Ann Rev Physiol* 64:899–923.
5. Praetorius J, Nejsum LN, Nielsen S (2004) *Am J Physiol Cell Physiol* 286:C601–C610.
6. Bouzinova EV, Praetorius J, Virkki LV, Nielsen S, Boron WF, Aalkjaer C (2005) *Am J Physiol Cell Physiol* 289:C1448–C1456.
7. Giffard RG, Lee YS, Ouyang YB, Murphy SL, Monyer H (2003) *Euro J Neurosci* 18:2935–2945.
8. Hübner CA, Hentschke M, Jacobs S, Hermans-Borgmeyer I (2004) *Gene Expr Patterns* 5:219–223.
9. Balestrino M, Somjen GG (1988) *J Physiol* 396:247–266.
10. Somjen GG, Tombaugh GC (1998) in *pH and Brain Function*, eds Kaila K, Ransom BR (Wiley, New York).
11. Schuchmann S, Schmitz D, Rivera C, Vanhatalo S, Salmen B, Mackie K, Sipilä ST, Voipio J, Kaila K (2006) *Nature Med* 12:817–823.
12. Hentschke M, Wiemann M, Hentschke S, Kurth I, Hermans-Borgmeyer I, Seidenbecher T, Jentsch TJ, Gal A, Hübner CA (2006) *Mol Cell Biol* 26:182–191.
13. Sander T, Toliat MR, Heils A, Leschik G, Becker C, Ruschendorf F, Rohde K, Mundlos S, Nurnberg P (2002) *Epilepsy Res* 51:249–255.
14. Xiong ZQ, Saggau P, Stringer JL (2000) *J Neurosci* 20:1290–1296.
15. Orlowski J, Grinstein S (1997) *J Biol Chem* 272:22373–22376.
16. Gamba G (2005) *Physiol Rev* 85:423–493.
17. Mount DB, Romero MF (2004) *Pflügers Arch* 447:710–721.
18. Hübner CA, Rust MB (2007) *Physiology of Cation–Chloride Cotransporters* (Elsevier, San Diego).
19. Blezer EL, Nicolay K, Viergever MA, Koomans HA, Joles JA (1999) *Magn Reson Imaging* 17:903–907.
20. Oshio K, Watanabe H, Song Y, Verkman AS, Manley GT (2005) *FASEB J* 19:76–78.
21. Deng QS, Johanson CE (1989) *Brain Res* 501:183–187.
22. Davson H, Luck CP (1957) *J Physiol* 137:279–293.
23. Davson H, Segal MB (1970) *J Physiol* 209:131–153.
24. Morgan PE, Pastorekova S, Stuart-Tilley AK, Alper SL, Casey JR (2007) *Am J Physiol Cell Physiol* 293:C738–C748.
25. Buzsaki G (1986) *Brain Res* 398:242–252.
26. Miles R, Wong RK (1983) *Nature* 306:371–373.
27. Traub RD, Wong RK (1982) *Science* 216:745–747.
28. Buzsaki G (2006) *Rhythms of the Brain* (Oxford Univ Press, London).
29. Sipilä ST, Kaila K (2008) *Results Probl Cell Differ* 44:99-121.
30. Escayg A, MacDonald BT, Meisler MH, Baulac S, Huberfeld G, An-Gourfinkel I, Brice A, LeGuern E, Moulard B, Chaigne D, *et al.* (2000) *Nature Gen* 24:343–345.
31. Heron SE, Crossland KM, Andermann E, Phillips HA, Hall AJ, Bleasel A, Shevell M, Mercho S, Seni MH, Guiot MC, *et al.* (2002) *Lancet* 360:851–852.
32. Kaila K, Voipio J (1987) *Nature* 330:163–165.
33. Kaila K (1994) *Prog Neurobiol* 42:489–537.
34. Kaila K, Voipio J, Paalasmaa P, Pasternack M, Deisz RA (1993) *J Physiol* 464:273–289.
35. Voipio J, Kaila K (2000) *Prog Brain Res* 125:329–338.
36. Ruusuvuori E, Li H, Huttu K, Palva JM, Smirnov S, Rivera C, Kaila K, Voipio J (2004) *J Neurosci* 24:2699–2707.
37. Lee J, Taira T, Pihlaja P, Ransom BR, Kaila K (1996) *Brain Res* 706:210–216.
38. Hübner CA, Stein V, Hermans-Borgmeyer I, Meyer T, Ballanyi K, Jentsch TJ (2001) *Neuron* 30:515–524.
39. Kurth I, Thompson DA, Ruther K, Feathers KL, Chrispell JD, Schroth J, McHenry CL, Schweizer M, Skosyrski S, Gal A, *et al.* (2007) *Mol Cell Biol* 27:1370–1379.
40. Boettger T, Rust MB, Maier H, Seidenbecher T, Schweizer M, Keating DJ, Faulhaber J, Ehmke H, Pfeffer C, Scheel O, *et al.* (2003) *EMBO J* 22:5422–5434.